ARTICLE OPEN

Check for updates

$NaRuO_2$: Kitaev-Heisenberg exchange in triangular-lattice setting

Pritam Bhattacharyya[1]✉, Nikolay A. Bogdanov[2], Satoshi Nishimoto[1,3], Stephen D. Wilson[4] and Liviu Hozoi[1]✉

Kitaev exchange, a new paradigm in quantum magnetism research, occurs for 90° metal-ligand-metal links, t_{2g}^5 transition ions, and sizable spin-orbit coupling. It is being studied in honeycomb compounds but also on triangular lattices. While for the former it is known by now that the Kitaev intersite couplings are ferromagnetic, for the latter the situation is unclear. Here we pin down the exchange mechanisms and determine the effective coupling constants in the t_{2g}^5 triangular-lattice material $NaRuO_2$, recently found to host a quantum spin liquid ground state. We show that, compared to honeycomb compounds, the characteristic triangular-lattice cation surroundings dramatically affect exchange paths and effective coupling parameters, changing the Kitaev interactions to antiferromagnetic. Quantum chemical analysis combined with subsequent effective spin model simulations provide perspective onto the nature of the experimentally observed quantum spin liquid—it seemingly implies fairly large antiferromagnetic second-neighbor isotropic exchange, and the atypical proximity to ferromagnetic order is related to ferromagnetic nearest-neighbor Heisenberg coupling.

npj Quantum Materials (2023)8:52; https://doi.org/10.1038/s41535-023-00582-7

INTRODUCTION

Exchange through 90° metal-ligand-metal bonds represents one of the limiting cases in (super)exchange theory[1,2]. In the simplest situation of half-filled *d*-metal orbitals, this geometry is associated with Heisenberg ferromagnetism. Away from half-filling and for degenerate orbitals, however, very intricate physics may arise, as pointed out by Jackeli and Khaliullin for t_{2g}^5 magnetic centers with sizable spin-orbit coupling: highly anisotropic effective interactions involving only (pseudo)spin components normal to the M_2L_2 square plaquette formed by two transition-metal (TM) ions and the two bridging ligands[3,4]. In crystals of NaCl type and derivative rhombohedral structures which imply three different possible orientations of the M_2L_2 plaquettes (see Fig. 1), this translates into directional dependence of the nearest-neighbor exchange: on differently oriented adjacent M_2L_2 units—i.e., normal to either *x*, *y*, or *z*—different components of the magnetic moments interact, either $\tilde{S}_i^x$ and $\tilde{S}_j^x$ (red arrows in Fig. 1b for *x*-type, normal to the *x*-axis plaquettes), $\tilde{S}_i^y$ and $\tilde{S}_k^y$ (blue arrows, *y*-type plaquettes), or $\tilde{S}_i^z$ and $\tilde{S}_l^z$ (green arrows, *z* type). The (super)exchange model of Jackeli and Khaliullin[3] thus formalizes Kitaev's effective Hamiltonian of bond-dependent anisotropic magnetic couplings[5] proposed initially more like a heuristic device. It launched a whole new subfield in the research area of quantum magnetic materials, that of $5d^5$ and $4d^5$ honeycomb magnets[4], with subsequent extension to $3d^7$ $t_{2g}^5e_g^2$ hexagonal networks of edge-sharing ML_6 octahedra.

Here we explore the nature of nearest-neighbor couplings in a $4d^5$ triangular-lattice magnet, $NaRuO_2$, and evidence the presence of sizable bond-dependent Kitaev interactions. Interestingly, those are antiferromagnetic, different from the case of honeycomb $4d^5$ and $5d^5$ magnetic lattices. Preliminary numerical tests highlight the important role of cation species around the ligands mediating (super)exchange: the sign change is related to electrostatics having to do with adjacent TM ions that in the honeycomb setting are missing. Sizable antiferromagnetic off-diagonal intersite couplings are also predicted, along with a somewhat larger ferromagnetic Heisenberg exchange. The latter seems to be consistent qualitatively with features seen in experiment: incipient ferromagnetism within a quantum-disordered ground state[6,7].

RESULTS

On-site multiplet structure and intersite couplings in $NaRuO_2$

$NaRuO_2$ is rather unique, a realization of $j_{\rm eff} \approx 1/2$ t_{2g}^5 moments on a triangular network of edge-sharing RuO_6 octahedra (see Fig. 2). The basic Ru^{3+} $4d^5$ multiplet structure in the specific delafossite crystalline setting of $NaRuO_2$ is illustrated in Table 1, as obtained by quantum chemical[8] complete-active-space self-consistent-field (CASSCF)[8,9] and post-CASSCF multireference configuration-interaction (MRCI)[8,10] embedded-cluster calculations (see Methods for computational details and Supplementary Note 1 for basis sets). To separately visualize the effects of crystal-field (CF) splittings and spin-orbit coupling (SOC), both scalar relativistic (CASSCF, MRCI) and MRCI+SOC[11] results are listed. The t_{2g}-e_g splitting is larger than in e.g., $RuCl_3$[12], due to larger ligand effective charges and shorter TM-ligand bonds in $NaRuO_2$. It is seen that the MRCI correlation treatment brings significant corrections to some of the CASSCF relative energies, in particular for the $^6A_{1g}$ term. Also important is the SOC (see the last two columns in Table 1). However, the effects of trigonal fields are visible too: those remove the degeneracy of the $^2T_{2g}$ CF states (*p*-orbital-like $l_{\rm eff} = 1/2$[13] and $s = 1/2$ quantum numbers in ideal cubic environment) and speak for significant deviations from textbook[3,13] $j_{\rm eff} = 1/2$ spin-orbit moments.

Even with sizable trigonal fields, existing estimates of several meV for the Kitaev interactions in honeycomb-lattice $4d$ t_{2g}^5 compounds such as $RuCl_3$ (see e.g.[12,14–19] and discussion in ref. [20]) and Li_2RhO_3[21] provide strong motivation for detailed ab initio investigation of the effective couplings in $NaRuO_2$. To this

[1]Institute for Theoretical Solid State Physics, Leibniz IFW Dresden, Helmholtzstraße 20, Dresden 01069, Germany. [2]Max Planck Institute for Solid State Research, Heisenbergstraße 1, Stuttgart 70569, Germany. [3]Department of Physics, Technical University Dresden, Dresden 01069, Germany. [4]Materials Department, University of California, Santa Barbara, CA 93106-5050, USA. ✉email: pritambhattacharyya01@gmail.com; l.hozoi@ifw-dresden.de

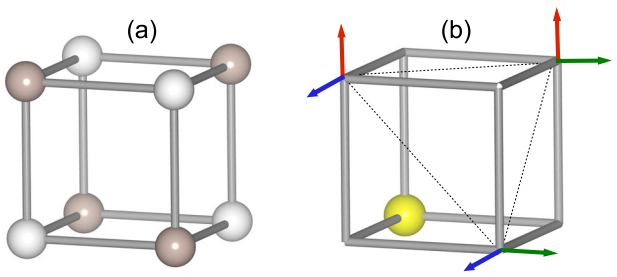

Fig. 1 Orthogonal M_2L_2 plaquettes in solids. a Rocksalt lattice, the prototype for 90° M-L-M exchange[1,2]. **b** If two different cation varieties—alkaline (*A*, yellow) and magnetic TM (*B*) ions—form successive layers normal to the [111] axis, a rhombohedral ABL_2 structure results, with a triangular network of edge-sharing octahedra (either AL_6 or BL_6) in each layer. On each B_2L_2 plaquette (atoms not explicitly shown), the Kitaev interaction couples only (pseudo)spin components perpendicular to the respective plaquette. Red, blue, and green indicate *x*, *y*, and *z* projections, respectively; only two spin components are shown at each magnetic site.

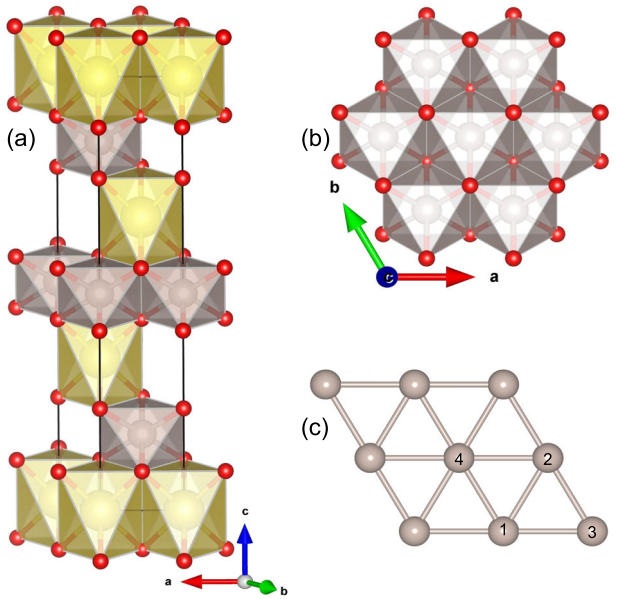

Fig. 2 $NaRuO_2$ crystal structure. a Sketch of successive layers of edge-sharing RuO_6 and NaO_6 octahedra. Gray, red, and yellow spheres represent Ru, O, and Na ions, respectively. **b** The triangular magnetic network of RuO_6 units. **c** To understand how the nearby surroundings affect magnetic couplings, Ru neighbors in the median plane (sites 3, 4) of a given Ru-Ru magnetic link (sites 1, 2) were removed in one set of quantum chemical computations.

end, further quantum chemical computations were performed for a block of two adjacent edge-sharing RuO_6 octahedra, following the procedure described in refs. [12,22] (see also Methods). Mapping the quantum chemical data onto the relevant effective spin model for C_{2h} symmetry of the $[Ru_2O_{10}]$ magnetic unit,

$$\mathcal{H}_{ij}^{(\gamma)} = J\tilde{\mathbf{S}}_i \cdot \tilde{\mathbf{S}}_j + K\tilde{S}_i^{\gamma}\tilde{S}_j^{\gamma} + \sum_{\alpha\neq\beta}\Gamma_{\alpha\beta}(\tilde{S}_i^{\alpha}\tilde{S}_j^{\beta} + \tilde{S}_i^{\beta}\tilde{S}_j^{\alpha}), \quad (1)$$

by spin-orbit MRCI, we arrive to Kitaev, Heisenberg, and off-diagonal Γ coupling constants $K = 2.0$, $J = -5.2$, $\Gamma \equiv \Gamma_{xy} = 3.6$, $\Gamma' \equiv \Gamma_{yz} = \Gamma_{zx} = 1.1$ (meV). Interestingly, both *K* and Γ are antiferromagnetic, with $\Gamma > K$, but the largest interaction parameter is the Heisenberg *J*. The latter being ferromagnetic, it brings us away from the antiferromagnetic ground states (zigzag antiferromagnetic order, in particular) experimentally found in $j \approx 1/2$ honeycomb systems, as

Table 1. $Ru^{3+}4d^5$ multiplet structure, with all five 4*d* orbitals active in CASSCF.

$Ru^{3+}4d^5$ splittings (eV)	CASSCF	MRCI	MRCI +SOC
$^2T_{2g}$ (t_{2g}^5)	0	0	0
	0.11	0.12	0.21
	0.11	0.12	0.26
$^4T_{1g}$ $(t_{2g}^4e_g^1)$	1.42	1.58	1.61
	1.45	1.62	|
	1.45	1.62	1.74
$^6A_{1g}$ $(t_{2g}^3e_g^2)$	1.42	1.91	2.08 (×3)
$^4T_{2g}$ $(t_{2g}^4e_g^1)$	2.16	2.28	2.37
	2.16	2.28	|
	2.20	2.30	2.42

Each MRCI+SOC value refers to a Kramers doublet (KD); just the lowest and highest KDs are shown for each group of $t_{2g}^4e_g^1$ spin-orbit states. Only the CF terms listed in the table entered the spin-orbit calculations. For simplicity, notations corresponding to O_h symmetry are used.

Table 2. Nearest-neighbor effective magnetic couplings (MRCI+SOC) for experimentally determined crystal structures of $NaRuO_2$/$RuCl_3$ and for adjusted configurations with modified median plane (MMP) cation distribution (see main text and Fig. 2c for details).

MRCI+SOC (meV)	*K*	*J*	Γ	Γ′
$NaRuO_2$	2.0	−5.2	3.6	1.1
$NaRuO_2$, MMP	−19	12	1.2	−1.1
$RuCl_3$[12]	−5.6	1.2	1.2	−0.7
$RuCl_3$, MMP	1.9	−12	1.1	−0.1

depicted for instance in the phase diagrams computed for *J*-*K*-Γ triangular-lattice models in ref. [23].

According to ref. [23], quantum spin liquid (QSL) ground states can only be realized for relatively large, antiferromagnetic Γ. Our result for the strength of Γ represents the largest ab initio quantum chemical estimate so far in a real material setting. Yet, a nearest-neighbor *J* that is even larger in magnitude and ferromagnetic (see the values listed above and at the top of Table 2) implies that only longer-range Heisenberg couplings (analyzed in isotropic context in e.g. refs. [24–27]) and/or higher-order interactions such as ring exchange[28–30] can pull the system to the QSL regime evidenced experimentally[6].

Signatures of a nearby ferromagnetic state in $NaRuO_2$ appear via the enhanced Van Vleck term in the magnetic susceptibility[6], which approaches values observed in nearly magnetic metals like Pd. Furthermore, despite possessing a charge gap and insulating ground state, clear quasiparticle excitations generate a Sommerfeld-like term in the low-temperature heat capacity[6]. This suggests the presence of strong spin fluctuations associated with a nearby magnetic state. These seemingly gapless spin fluctuations are robust, and are directly resolved in neutron scattering as diffuse continuum-like modes about the nuclear zone center and near $\mathbf{Q} = 0$[6]. Initial attempts at scaling S(Q, E) suggest the proximity of a nearby ferromagnetic quantum critical point, and small, nonmagnetic chemical perturbations to the network of Ru^{3+} ions induce glass-like freezing of the magnetic moments[7].

What makes *K* antiferromagnetic

Finding an antiferromagnetic Kitaev coupling in $NaRuO_2$, opposite to the ferromagnetic *K* generally found in honeycomb Kitaev-

Heisenberg magnets (see[12,21,31] for quantum chemical results, refs. [14–17] for estimates based on effective-model (super)exchange theory, and refs. [18,19] for values obtained by fitting experimental spectra) is intriguing. To shed light on this aspect, we performed the following numerical experiment: in a new set of quantum chemical computations, the two magnetic-plane cations in the immediate neighborhood of the bridging ligands, forming a line perpendicular to the link of nearest-neighbor Ru sites (see Fig. 2c), were removed and their charge redistributed within the point-charge array modeling the extended solid-state surroundings. Remarkably, without those nearby positive ions, three of the effective magnetic couplings change sign (see Table 2). This suggests that strong orbital polarization effects at the ligand sites, induced by the extra nearby positive charge on the triangular lattice (+3 effective nearby charges in $NaRuO_2$ versus +1 in honeycomb '213' compounds such as Na_2IrO_3 and Li_2RhO_3 or 0 in $RuCl_3$) have dramatic consequences on hopping matrix elements and superexchange processes. Similar additional tests for $RuCl_3$, where +3 ions were placed in the centers of two edge-sharing Ru_6 hexagonal rings, confirm the trend: the extra positive charge in the neighborhood of the Ru_2O_2 'magnetic' plaquette (i.e., $[Ru_2O_{10}]$ cluster of edge-sharing octahedra) invert the sign of the Kitaev coupling constant, from ferromagnetic in actual $RuCl_3$[12] to antiferromagnetic in the presence of positive charge in the centers of the two hexagons sharing the magnetic Ru-Ru link (see lowest lines in Table 2). Strong polarization effects of this type were earlier pointed out in the case of the Kitaev-Heisenberg honeycomb iridate $H_3LiIr_2O_6$[31], produced in that case by cations residing between the magnetic layers.

Ru_2O_2-unit correlations. Extended magnetic lattice

Insights into the interplay between spin-orbit couplings and electron correlation effects on a plaquette of two nearest-neighbor Ru ions and two bridging ligands can be obtained by analyzing computational data obtained at lower levels of approximation, i.e., spin-orbit calculations including only the t_{2g}^5–t_{2g}^5 electron configuration and CASSCF+SOC calculations that also account for excited-state t_{2g}^4–t_{2g}^6 configurations since all possible occupations are considered within the six-orbital (three t_{2g} orbitals per Ru site) active space in the latter case.

As illustrated in Table 3, anisotropic effective intersite interactions comparable in size with the isotropic Heisenberg J are already found at the single-configuration (SC) level, i.e., when accounting for just t_{2g}^5–t_{2g}^5 Coulomb exchange (sometimes referred to as direct exchange[2]). Large anisotropic Coulomb exchange as found in the SC calculation represents physics not addressed so far in the literature—Kitaev magnetism is presently exclusively explained through TM-TM kinetic exchange and TM-L-TM superexchange.

CASSCF, through the inclusion of intersite $t_{2g}\rightarrow t_{2g}$ excitations (i.e., TM-TM kinetic exchange), brings sizable corrections to K, J, and Γ in particular. By considering next, in the spin-orbit MRCI treatment, all possible single and double excitations out of the Ru t_{2g} and bridging-ligand orbitals (Ru(t_{2g})→Ru(e_g) and O(2p)→Ru(4d) transitions, among others), the most significant post-CASSCF corrections are found to occur for K and Γ. This suggests that more sophisticated calculations, e.g., MRCI+SOC based on larger active spaces in the prior CASSCF, would bring significant additional corrections to K and Γ mostly, i.e., would only enhance antiferromagnetic fluctuations on the extended lattice.

Table 3. Nearest-neighbor magnetic couplings (meV) at different levels of theory: SC (only the t_{2g}^5–t_{2g}^5 configuration considered), CASSCF (also t_{2g}^4–t_{2g}^6 states included), and MRCI (single and double excitations out of the Ru 4d t_{2g} and bridging-O 2p levels on top of CASSCF).

Magnetic couplings	K	J	Γ	Γ′
SC+SOC	−1.0	−0.7	0.4	0.8
CASSCF+SOC	1.3	−5.2	2.2	1.0
MRCI+SOC	2.0	−5.2	3.6	1.1

An interesting observation is that, adding the Coulomb-exchange contributions computed at SC level for K and J (−1.0 and −0.7 meV, respectively, first line in Table 3) to the K and J estimates derived from effective-model calculations where Coulomb exchange is neglected ($K = 2.9$ and $J = -4.2$ meV)[32] brings the latter in rather good agreement with the MRCI values (2.0 and −5.2 meV, respectively), although this is not the case for Γ and Γ′.

To obtain first impressions on the role of longer-range Heisenberg interactions, second-neighbor (J_2) and third-neighbor (J_3), in particular, we performed density-matrix renormalization group (DMRG) calculations[33,34] for a J-K-Γ-Γ′-J_2-J_3 model on fragments of 19, 27, and 37 sites of the triangular lattice. In order to prevent artifacts, e.g., artificial stabilization (or destabilization) of particular magnetic states, we applied open boundary conditions. The validity of this material model is discussed in Supplementary Note 2 and Supplementary Note 3. Setting J, K, Γ, and Γ′ to –5.5, 4, 4, and 1.5 meV, respectively, we obtain a very rich phase diagram, see Fig. 3. Notably, a QSL phase is found for antiferromagnetic J_2 values and ferromagnetic J_3. The corresponding structure factor has no Bragg peaks but exhibits a characteristic pattern. It indicates that the QSL emerges from the competition of adjacent ordered states. The most remarkable spot is the region where the QSL neighbors ferromagnetic order and a spiral phase, namely, around $J_2 = 5$, $J_3 = -2$—as shown in Fig. 3, at $J_2 = 5$, $J_3 = -2$ the structure factor implies a broad spectral feature for momenta near $|\mathbf{Q}| = 0$, seemingly consistent with experimental observations[6].

DISCUSSION

While the way nearby cations are structurally arranged can strongly affect on-site electronic-structure features such as subshell level splittings[22,35,36], single-ion anisotropies[35], and g factors[22,36], detailed ab initio investigations of the effect on intersite magnetic couplings are less numerous. Here we show that, compared to honeycomb compounds, the characteristic triangular-lattice cation surroundings dramatically affect superexchange paths and effective coupling parameters. In particular, with respect to honeycomb $j \approx 1/2$ systems, the Kitaev interaction constant changes its sign in triangular-lattice $NaRuO_2$. By providing insight into the signs and strengths of the nearest-neighbor magnetic interactions in this material, our work sets the frame within which the role of longer-range effective spin couplings should be addressed. Interestingly, while giving rise to antiferromagnetic order on honeycomb Kitaev-Heisenberg lattices, the latter appear to be decisive in realizing quantum disorder[6] in $NaRuO_2$. Last but not least, we establish the role of anisotropic Coulomb exchange (in trianguar-lattice setting), a mechanism not addressed so far in Kitaev-Heisenberg magnetism.

METHODS

Ru-site multiplet structure

All quantum chemical computations were carried out using the MOLPRO suite of programs[37]. Crystallographic data as reported by Ortiz et al.[6] were utilized. For each type of embedded cluster, the crystalline environment was modeled as a large array of point charges which reproduces the crystalline Madelung field within the cluster volume; we employed the EWALD program[38,39] to generate the point-charge embeddings.

To clarify the Ru-site multiplet structure, a cluster consisting of one 'central' RuO_6 octahedron, the six in-plane adjacent

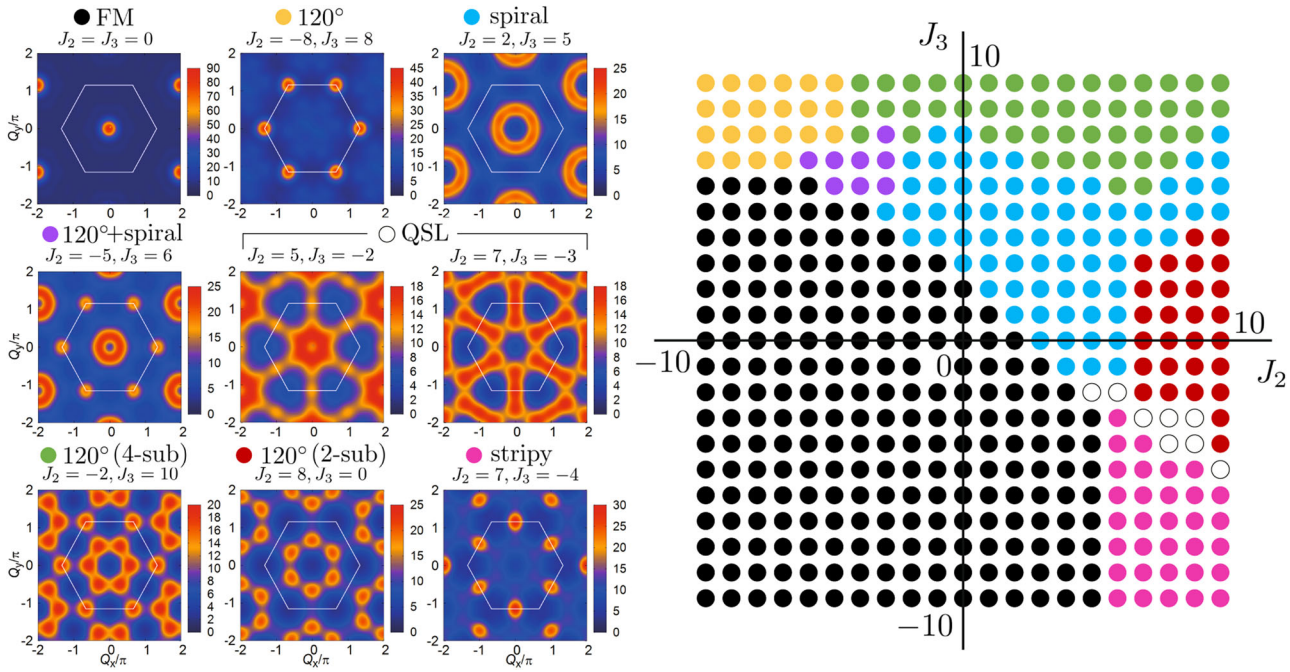

Fig. 3 Single-layer magnetism. Ground-state phase diagram obtained by DMRG computations for the J-K-Γ-Γ′-J_2-J_3 model (right) and typical static spin structure factors for each phase (left). Using the quantum chemical analysis as a guide (see data in Table 3 and related discussion), J, K, Γ, and Γ′ were set to to −5.5, 4, 4, and 1.5 meV, respectively.

octahedra, and 12 nearby Na cations was designed. The quantum chemical study was initiated as CASSCF calculations[8,9] with an active orbital space containing the five 4*d* orbitals of the central Ru ion. Post-CASSCF correlation computations were performed at the MRCI level, with single and double excitations[8,10] out of the Ru 4*d* and O 2*p* orbitals of the central RuO_6 octahedron. SOCs were accounted for following the procedure described in ref. [11].

Intersite exchange in $NaRuO_2$

Clusters with two edge-sharing RuO_6 octahedra in the central region were considered in order to derive the intersite effective magnetic couplings. The eight in-plane octahedra directly linked to the two-octahedra central unit and 22 nearby Na ions were also explicitly included in the quantum chemical computations but using much more compact basis sets.

CASSCF computations were carried out with six (Ru t_{2g}) valence orbitals and ten electrons as active (abbreviated as (10e,6o) active space); the t_{2g} orbitals of the adjacent TM ions were part of the inactive orbital space. In the subsequent MRCI correlation treatment, single and double excitations out of the central-unit Ru t_{2g} and bridging-O 2*p* levels were considered. We used the Pipek-Mezey methodology[40] to obtain localized central-unit orbitals.

The CASSCF optimization was performed for the lowest nine singlet and lowest nine triplet states associated with the (10e,6o) setting. Those were the states for which SOCs were further accounted for[11], either at SC, CASSCF, or MRCI level, which finally yields a number of 36 spin-orbit states in each case. The SC label in Table 3 in the main text stands for a CASCI in which intersite excitations are not considered. This is also referred to as occupation-restricted multiple active space (ORMAS) scheme[41].

The lowest four spin-orbit eigenstates from the MOLPRO output (eigenvalues lower by ~200 meV or more than the eigenvalues of higher-lying excited states, as illustrated for example in Table 1) were mapped onto the eigenvectors of the effective spin Hamiltonian (1), following the procedure described in refs. [12,22]: those four expectation values and the matrix elements of the Zeeman Hamiltonian in the basis of the four lowest-energy spin-orbit eigenvectors are put in direct correspondence with the respective eigenvalues and matrix elements of (1). Having two of the states in the same irreducible representation of the C_{2h} point group[21], such one-to-one mapping translates into two possible sets of effective magnetic couplings. The relevant array is chosen as the one whose g factors fit the g factors obtained for a single $RuO_6 t_{2g}^5$ octahedron.

We used the standard coordinate frame usually employed in the literature, different from the rotated frame employed in earlier quantum chemical studies[12,21,31] that affects the sign of Γ. This is the reason the sign of Γ for $RuCl_3$ in Table 2 in the main text is different from the sign in ref. [12] (see also footnote [48] in ref. [20]).

DATA AVAILABILITY

Quantum chemical data (atomic coordinates, point-charge data, MOLPRO output) have been deposited in the RADAR database under the https://doi.org/10.22000/1736.

CODE AVAILABILITY

Relevant codes are available from the corresponding author upon reasonable request.

Received: 18 April 2023; Accepted: 13 September 2023;
Published online: 02 October 2023

REFERENCES

1. Kanamori, J. Superexchange interaction and symmetry properties of electron orbitals. *J. Phys. Chem. Solids* **10**, 87 (1959).
2. Anderson, P. W. New approach to the theory of superexchange interactions. *Phys. Rev.* **115**, 2 (1959).
3. Jackeli, G. & Khaliullin, G. Mott insulators in the strong spin-orbit coupling limit: from heisenberg to a quantum compass and kitaev models. *Phys. Rev. Lett.* **102**, 017205 (2009).
4. Takagi, H., Takayama, T., Jackeli, G., Khaliullin, G. & Nagler, S. E. Concept and realization of kitaev quantum spin liquids. *Nat. Rev. Phys.* **1**, 264 (2019).

5. Kitaev, A. Anyons in an exactly solved model and beyond. *Ann. Phys.* **321**, 2 (2006).
6. Ortiz, B. R. et al. Quantum disordered ground state in the triangular-lattice magnet $NaRuO_2$. *Nat. Phys.* **19**, 943 (2023).
7. Ortiz, B. R., Sarte, P. M., Avidor, A. H. & Wilson, S. D. Defect control in the heisenberg-kitaev candidate material $NaRuO_2$. *Phys. Rev. Mater.* **6**, 104413 (2022).
8. Helgaker, T., Jørgensen, P. and Olsen, J. Molecular electronic structure theory (John Wiley & Sons, Chichester, 2000).
9. Kreplin, D. A., Knowles, P. J. & Werner, H.-J. MCSCF optimization revisited. II. combined first- and second-order orbital optimization for large molecules. *J. Chem. Phys.* **152**, 074102 (2020).
10. Knowles, P. J. & Werner, H.-J. Internally contracted multiconfiguration-reference configuration interaction calculations for excited states. *Theor. Chim. Acta* **84**, 95 (1992).
11. Berning, A., Schweizer, M., Werner, H.-J., Knowles, P. J. & Palmieri, P. Spin-orbit matrix elements for internally contracted multireference configuration interaction wavefunctions. *Mol. Phys.* **98**, 1823 (2000).
12. Yadav, R. et al. Kitaev exchange and field-induced quantum spin-liquid states in honeycomb α-$RuCl_3$. *Sci. Rep.* **6**, 37925 (2016).
13. Abragam, A. and Bleaney, B. Electron Paramagnetic Resonance of Transition Ions (Clarendon Press, Oxford, 1970).
14. Kim, H.-S. & Kee, H.-Y. Crystal structure and magnetism in α-$RuCl_3$: An ab initio study. *Phys. Rev. B* **93**, 155143 (2016).
15. Winter, S. M., Li, Y., Jeschke, H. O. & Valenti, R. Challenges in design of kitaev materials: Magnetic interactions from competing energy scales. *Phys. Rev. B* **93**, 214431 (2016).
16. Wang, W., Dong, Z.-Y., Yu, S.-L. & Li, J.-X. Theoretical investigation of magnetic dynamics in α-$RuCl_3$. *Phys. Rev. B* **96**, 115103 (2017).
17. Eichstaedt, C. et al. Deriving models for the kitaev spin-liquid candidate material α-$RuCl_3$ from first principles. *Phys. Rev. B* **100**, 075110 (2019).
18. Li, H. et al. Identification of magnetic interactions and high-field quantum spin liquid in α-$RuCl_3$. *Nat. Commun.* **12**, 4007 (2021).
19. Samarakoon, A. M. et al. Extraction of interaction parameters for α-$RuCl_3$ from neutron data using machine learning. *Phys. Rev. Res.* **4**, L022061 (2022).
20. Janssen, L., Andrade, E. C. & Vojta, M. Magnetization processes of zigzag states on the honeycomb lattice: Identifying spin models for α-RuCl and Na_2IrO_3. *Phys. Rev. B* **96**, 064430 (2017).
21. Katukuri, V. M. et al. Strong magnetic frustration and anti-site disorder causing spin-glass behavior in honeycomb Li_2RhO_3. *Sci. Rep.* **5**, 14718 (2015).
22. Bogdanov, N. A. et al. Orbital reconstruction in nonpolar tetravalent transition-metal oxide layers. *Nat. Commun.* **6**, 7306 (2015).
23. Wang, S. et al. Comprehensive study of the global phase diagram of the $J-K-\Gamma$ model on a triangular lattice. *Phys. Rev. B* **103**, 054410 (2021).
24. Mishmash, R. V., Garrison, J. R., Bieri, S. & Xu, C. Theory of a competitive spin liquid state for weak mott insulators on the triangular lattice. *Phys. Rev. Lett.* **111**, 157203 (2013).
25. Zhu, Z. & White, S. R. Spin liquid phase of the $S=\frac{1}{2}J_1-J_2$ Heisenberg model on the triangular lattice. *Phys. Rev. B* **92**, 041105 (2015).
26. Iqbal, Y., Hu, W.-J., Thomale, R., Poilblanc, D. & Becca, F. Spin liquid nature in the heisenberg J_1–J_2 triangular antiferromagnet. *Phys. Rev. B* **93**, 144411 (2016).
27. Hu, S., Zhu, W., Eggert, S. & He, Y.-C. Dirac spin liquid on the spin-1/2 triangular heisenberg antiferromagnet. *Phys. Rev. Lett.* **123**, 207203 (2019).
28. Motrunich, O. I. Variational study of triangular lattice spin-1/2 model with ring exchanges and spin liquid state in k-$(ET)_2Cu_2(CN)_3$. *Phys. Rev. B* **72**, 045105 (2005).
29. Cookmeyer, T., Motruk, J. & Moore, J. E. Four-spin terms and the origin of the chiral spin liquid in mott insulators on the triangular lattice. *Phys. Rev. Lett.* **127**, 087201 (2021).
30. Zhao, Q.-R. & Liu, Z.-X. Thermal properties and instability of a U(1) spin liquid on the triangular lattice. *Phys. Rev. Lett.* **127**, 127205 (2021).
31. Yadav, R. et al. Engineering kitaev exchange in stacked iridate layers: impact of inter-layer species on in-plane magnetism. *Chem. Sci.* **10**, 1866 (2019).
32. Razpopov, A. et al. A $j_{\text{eff}}=1/2$ kitaev material on the triangular lattice: the case of $NaRuO_2$. *npj Quantum Mater.* **8**, 36 (2023).
33. White, S. R. Density matrix formulation for quantum renormalization groups. *Phys. Rev. Lett.* **69**, 2863 (1992).
34. Fishman, M., White, S. R. and Stoudenmire, E. M. The ITensor Software Library for Tensor Network Calculations, https://doi.org/10.21468/SciPostPhysCodeb.4 *SciPost Phys. Codebases*, 4 (2022).
35. Bogdanov, N. A., Maurice, R., Rousochatzakis, I., van den Brink, J. & Hozoi, L. *Phys. Rev. Lett.* **110**, 127206 (2013).
36. Zangeneh, Z., Avdoshenko, S., van den Brink, J. & Hozoi, L. Single-site magnetic anisotropy governed by interlayer cation charge imbalance in triangular-lattice $AYbX_2$. *Phys. Rev. B* **100**, 174436 (2019).
37. Werner, H.-J., Knowles, P. J., Knizia, G., Manby, F. R. & Schütz, M. Molpro: a general-purpose quantum chemistry program package. *WIREs Comput. Mol. Sci.* **2**, 242 (2012).
38. Klintenberg, M., Derenzo, S. E. & Weber, M. J. Accurate crystal fields for embedded cluster calculations. *Comp. Phys. Commun.* **131**, 120 (2000).
39. Derenzo, S. E., Klintenberg, M. K. & Weber, M. J. Determining point charge arrays that produce accurate ionic crystal fields for atomic cluster calculations. *J. Chem. Phys.* **112**, 2074 (2000).
40. Pipek, J. & Mezey, P. G. A fast intrinsic localization procedure applicable for ab initio and semiempirical linear combination of atomic orbital wave functions. *J. Chem. Phys.* **90**, 4916 (1989).
41. Ivanic, J. Direct configuration interaction and multiconfigurational self-consistent-field method for multiple active spaces with variable occupations. I. Method. *J. Chem. Phys.* **119**, 9364 (2003).

ACKNOWLEDGEMENTS

P. B. and L. H. acknowledge financial support from the German Research Foundation (Deutsche Forschungsgemeinschaft, DFG), Project ID 441216021, and technical assistance from U. Nitzsche. S. N. acknowledges financial support via project A05 of the Collaborative Research Center 1143 of the DFG (Project ID 247310070). S. D. W. acknowledges support via DOE, Office of Science, Basic Energy Sciences under Award DE-SC0017752. P. B. thanks M. S. Eldeeb for discussions. We also acknowledge instructive discussions with I. Rousochatzakis, U. K. Rößler, and G. Khaliullin.

AUTHOR CONTRIBUTIONS

P.B. performed the ab initio quantum chemical computations, with assistance from L.H. and N.A.B. S.N. carried out the model-Hamiltonian calculations for the extended lattice and subsequent analysis. S.D.W. and L.H. initiated this study.

FUNDING

Open Access funding enabled and organized by Projekt DEAL.

COMPETING INTERESTS

The authors declare no competing interests.

ADDITIONAL INFORMATION

Supplementary information The online version contains supplementary material available at https://doi.org/10.1038/s41535-023-00582-7.

Correspondence and requests for materials should be addressed to Pritam Bhattacharyya or Liviu Hozoi.

Reprints and permission information is available at http://www.nature.com/reprints

Publisher's note Springer Nature remains neutral with regard to jurisdictional claims in published maps and institutional affiliations.